# ROBUST TECHNIQUES FOR BUILDING FOOTPRINT EXTRACTION IN AERIAL LASER SCANNING 3D POINT CLOUDS

A. Nurunnabi[1] [*], N. Teferle[1], J. Balado[2], M. Chen[3], F. Poux[4], C. Sun[5]

[1] Geodesy and Geospatial Engineering, Faculty of Science, Technology and Medicine, University of Luxembourg
6, rue Richard Coudenhove-Kalergi, L-1359 Luxembourg, − (abdul.nurunnabi, norman.teferle)@uni.lu
[2] CINTECX, GeoTECH Group, University of Vigo, 36310 Vigo, Spain,− jbalado@uvigo.es
[3] Institute for Creative Technologies, University of Southern California, Los Angeles, CA 90094, USA,− mechen@ict.usc.edu
[4] Geomatics Unit, Faculty of Science, University of Liège, Allée du 7 Août, 4000 Liège, Belgium,− fpoux@uliege.be
[5] School of Mathematical and Geospatial Sciences, RMIT University, Melbourne, VIC 3000, Australia,− chayn.sun@rmit.edu.au

**KEY WORDS:** Building Modeling, Classification, Digital Twins, Feature Extraction, Robust Regression, Semantic Segmentation

**ABSTRACT:**

The building footprint is crucial for a volumetric 3D representation of a building that is applied in urban planning, 3D city modeling, cadastral and topographic map generation. Aerial laser scanning (ALS) has been recognized as the most suitable means of large-scale 3D point cloud data (PCD) acquisition. PCD can produce geometric detail of a scanned surface. However, it is almost impossible to get point clouds without noise and outliers. Besides, data incompleteness and occlusions are two common phenomena for PCD. Most of the existing methods for building footprint extraction employ classification, segmentation, voting techniques (e.g., Hough-Transform or RANSAC), or Principal Component Analysis (PCA) based methods. It is known that classical PCA is highly sensitive to outliers, even RANSAC which is known as a robust technique for shape detection is not free from outlier effects. This paper presents a novel algorithm that employs MCMD (maximum consistency within minimum distance), MSAC (a robust variant of RANSAC) and a robust regression to extract reliable building footprints in the presence of outliers, missing points and irregular data distributions. The algorithm is successfully demonstrated through two sets of ALS PCD.

## 1. INTRODUCTION

A volumetric three-dimensional (3D) representation, i.e., a 3D model of a building has many applications involved in urban planning, energy and property management, cadastral extraction, topographic map generation, understanding of 3D GIS applications and many of the location-based services (Rau and Lin, 2011; Yang et al., 2013; Zhao et al., 2021, Nurunnabi et al., 2016b) that largely underpins the development of urban digital twins by providing large-scale 3D city model (Park and Guldmann, 2019; Dimitrov and Petrova-Antonova, 2021). In this setting, building footprint extraction plays a substantial role to generate a building model. Although there is a lack of consensus among the stakeholders/researchers in different countries to define building footprint, generally, a building footprint is a sketch that permit to infer the area of a building from the surface of the external walls of the building. This virtuously refers to the ground area utilized by construction. Hence, a building footprint can be extracted based on the data collected for the outer surface of the exterior walls (Chen et al., 2020).

Optical imagery and LiDAR (Light Detection and Ranging) based point clouds are the two main data sources used for building footprint extraction (Nex et al., 2013; Ebrahimi et al., 2017; Park and Guldmann, 2019; Schuegraf and Bittner, 2019). Nex et al (2013) used oblique imagery to generate dense point clouds and to find building footprints. Schuegraf and Bittner (2019) extracted building footprints using multi-resolution remote sensing images. Generally, many algorithms have been developed over the decades using LiDAR point clouds (Yang et al., 2013; Widyaningrum et al., 2019). LiDAR systems typically utilize laser light, which is projected on the object surface and its reflected backscattering is captured, where the structure of the object surface is determined following the time-of-flight principle and produces 3D point clouds (Campbell and Wynne,

2011). The main advantage of using point clouds over images is that they can produce geometric detail (e.g., height, position, and orientation information) with centimeter-level accuracy of a scanned object. Aerial LiDAR scanning (ALS) has been recognized as the fast and most cost-effective means of large-scale 3D point cloud data (PCD) acquisition system for surveying urban scenes. However, data incompleteness and irregular point distributions are two common phenomena for ALS point clouds that have detrimental effects on feature extraction. Data gaps occur mainly due to the occlusions caused by neighboring buildings, vegetation, parked vehicles, etc. Besides, it is almost impossible to get point clouds without noise and outliers (Nurunnabi et al., 2012; 2015). Hence, building footprint extraction using PCD has more potential than images but is very challenging. Most of the existing methods for building footprint extraction employ classification, pixel- and building- wise segmentation, edge detection (Dalitz et al., 2017), RANSAC (Neidhert and Sester, 2008), Hough-Transform (HT; Widyaningrum et al., 2019), photometric, structural and contextual analysis (Zeng et al., 2013).

Many researchers, who deal with ALS data, extract building footprints based on the building roof surface information (Awrangjeb and Lu, 2014; Chen et al., 2020), because extracting roof surface is easier than identifying building walls due to significantly higher point density and almost complete surface. They first identify roof surfaces and their boundaries, and then project them onto a 2D plane to get building footprints. Awrangjeb and Lu (2014) developed a segmentation-based approach to segment roof surfaces and then used corner-boundary detection algorithms to extract footprint. But projecting the roof surface onto the 2D planes may overestimate the building footprint because roof boundaries and outer walls are not always in the same direction and many of the buildings' exterior walls are within the roof boundaries. Instead of using the

---

* Corresponding author

traditional roof outline-based footprint extraction approach, some studies focused on using building exterior walls/facades information to generate footprints. Yang et al. (2013) developed a facades-based method, the authors used RANSAC for facades plane detection and Principal Component Analysis (PCA) to determine the facades directions. It has been shown that classical PCA is highly sensitive to noise and outliers, even RANSAC which is known as a robust technique for shape detection is not free from outlier effects (Nurunnabi et al., 2015; 2016a, b). HT is a well-known procedure for line feature extraction. Widyaningrum et al. (2019) pointed out that HT-based approaches have lack the flexibility to extract outlines for arbitrary buildings. The authors (Widyaningrum et al., 2019) developed an automatic building outline extraction method by ordered points aided HT.

Recently, deep neural network architecture, namely deep learning (DL) has been introduced in building footprint extraction. Schuegraf and Bittner (2019) proposed a U-shaped DL that merges depth (alternative to height) and spectral information for building footprint extraction. Sun et al. (2021) developed a frame field learning framework to extract building polygons using aerial imagery and the elevation data derived from the normalized digital surface model (nDSM). Zhao et al. (2021) developed a method that predicted building outline within an end-to-end DL framework. Buyukdemircioglu et al. (2022) developed a DL-based approach using red-green-blue (RGB), true orthophotos and digital surface model data. Mohamed et al. (2022) developed a Mask R-CNN (a region-based convolutional neural network, He et al., 2017) method for building footprint extraction in a dense urban area using LiDAR point clouds.

Zeng et al. (2013) pointed out that methods for building footprint extraction are not 100% successful, and it is almost impossible to reach that level, the reasons behind the deficiency are scene complexity, the complex architecture of the buildings, incomplete cue extraction, and sensor dependency.

This paper concentrates on the problems of buildings footprint extraction using classical techniques in the presence of outliers, missing points, and irregular data distributions in ALS point clouds. We present a novel algorithm that employs MCMD (maximum consistency within minimum distance; Nurunnabi et al., 2015), MSAC (a robust variant of RANSAC; Torr and Zisserman, 2000) and robust regression (Rousseeuw and Leroy, 2003; Nurunnabi et al., 2016a) algorithms to extract robust and reliable building footprints. The algorithm is successfully demonstrated through two sets of ALS PCD.

The remainder of the paper is arranged as follows. Section 2 briefly recaps the basic principles and methods used in the proposed algorithm in Section 3. Section 4 demonstrates the algorithm through two sets of real-world ALS point clouds. Finally, conclusions are drawn in Section 5.

## 2. RELATED PRINCIPLES AND METHODS

This section presents a brief discussion of methods and principles that are used in the new algorithm.

### 2.1 RandLA-Net

Many DL-based semantic segmentation algorithms exist in the literature that directly process PCD through neural network architectures (Qi et al., 2017; Thomas et al., 2019; Hu et al., 2020; Nurunnabi et al., 2021). Hu et al. (2020) developed the

RandLA-Net, a DL algorithm for semantic segmentation, which utilizes random point sampling for sub-sampling, follows an encoder-decoder architecture, and couples with a novel local feature aggregation module. This algorithm is memory efficient and fast that is capable to process large-scale 3D PCD in a single pass. The use of the local feature aggregation module progressively increases the receptive field size to preserve the complex geometric structure. The authors (Hu et al., 2020) demonstrated that the RandLA-Net is significantly faster than many state-of-the-art segmentation algorithms. We select RandLA because it was designed for large outdoor environments, large-scale ALS point clouds can be fitted into this architecture for efficient segmentation of building and ground points which is important for this study.

### 2.2 Maximum Consistency within Minimum Distance (MCMD)

PCA is a statistical technique often used to explain the covariance structure of a dataset and has been used in point cloud processing. Unfortunately, the covariance matrix that is used in PCA to be decomposed is sensitive to outliers, and so normals and other saliency features that are based on PCA are non-robust (Nurunnabi et al., 2014). Nurunnabi et al. (2015) proposed an outlier detection algorithm that finally generated robust local saliency features (normals and curvature) in the presence of outliers and noise. To identify outliers within a local neighborhood, this algorithm uses the point to plane orthogonal distance (OD) and the surface point variation (the value of the 3rd eigenvalue that is available in PCA) along the normal. Only the majority ($h = \lceil 0.5k \rceil$, $k$ is the neighborhood size) of points in a neighborhood that have the minimum sorted ODs are used to fit a plane by using PCA. This fitting process repeats a number of times to get the most consistent set that have the least 3rd eigenvalue, and the point set that has the least local surface point consistency. This criterion is referred to as the Maximum Consistency within a Minimum Distance (MCMD). The algorithm finally identifies outliers that have remarkably large robust Z-score, $Rz_i$

$$Rz_i = \frac{|OD_i - median\,(OD_j)|}{MAD(OD)}, \tag{1}$$

where $OD_i$ is the point to plane orthogonal distance for the $i$th point of interest in the local neighborhood, and MAD (OD) is defined as the median absolute deviation of the ODs of the point's local neighbors. After removing the outlying points, we get an outlier-free neighborhood that is finally used by PCA to estimate the required robust normals or other saliency features. Please refer to the original paper (Nurunnabi et al., 2015) for more detail about the MCMD algorithm.

### 2.3 RANSAC and MSAC

Random SAmple Consensus (RANSAC; Fischler and Bolles, 1981) is widely applied for robust estimation of various models' parameters. In operation, RANSAC finds the minimum of a cost function (C), defined as:

$$C = \sum_i \rho(e_i^2), \tag{2}$$

where $e_i$ is the error term of the $i$th observation, and

$$\rho\,(e^2) = \begin{cases} o & e^2 < T^2 \\ constant & e^2 \geq T^2 \end{cases}. \tag{3}$$

One of the limitations of RANSAC is that if the threshold (T) for

finding outliers is not defined properly, the estimation may not be robust. Literature shows many variants of RANSAC have been developed based on various cost functions (Choi et al., 2009). Torr and Zisserman (2000) developed an *m*-estimator sample consensus (MSAC), where the robust error term $\rho$ is defined as:

$$\rho \left(e^2\right) = \begin{cases} e^2 & e^2 < T^2 \\ T^2 & e^2 \geq T^2 \end{cases}, \tag{4}$$

which is simply a redescending M estimator, and $T = 1.96\sigma$. The authors (Torr and Zisserman, 2000) claimed that MSAC yields a modest to hefty benefit to all robust estimations without any computational burden.

### 2.4 Least Trimmed Square (LTS) regression

Classical least square (LS) regression fits a line by minimizing the sum of the squared residuals. It is known that the LS regression is sensitive to outliers and noise. One of the most popular robust linear regression approaches is the Least Trimmed Squares (LTS) regression (Rousseeuw and Leroy, 2003). To reduce the influence of outliers, typically robust regression fits a regression model to the majority of the data that have small residual values. LTS regression ignores the largest (*n*-*h*) residuals when it fits a line by minimizing the sum of the *h* lowest squared residuals, i.e.,

$$minimize_{\hat{\beta}} = \sum_i^h r_i^2, \tag{5}$$

where $r_1^2 \leq r_2^2 \leq \cdots r_i^2 \leq \cdots \leq r_h^2 \ldots \leq r_n^2$ are the ordered squared residuals, *h* is approximately *n*/2, *n* is the number of points in the data set, and $\beta$ is the parameter-vector. The highest possible breakdown point for the LTS regression is 50% (Rousseeuw and Leroy, 2003).

## 3. PROPOSED METHODOLOGY

This section proposes an algorithm based on robust techniques to extract building footprints from ALS data. Our method starts from the point-wise classified/labelled (semantically segmented) ALS point clouds, where building points are pre-identified and separated based on a reliable point-wise classification algorithm with minimum manual corrections. We employ a deep learning (DL) based semantic segmentation algorithm, RandLA-Net (Hu et al., 2020), which is efficient for segmenting large-scale urban PCD. The DL method can produce very good results, saves huge time, labour and cost, but does not guarantee 100% accuracy of segmentation. To achieve the best performance in the latter process, it is recommended to manually correct the miss-segmented (labelled) points. The proposed algorithm performs the following five sequential steps to extract building footprints. The flowchart for the proposed algorithm is shown in Fig. 1.

### 3.1 Step 1: Vertical and non-vertical surfaces separation

First, the building points are isolated into vertical (e.g., building wall points) and non-vertical surface points (e.g., roof points). We use points' slope (verticality) information, which is defined in Balado et al. (2018) as the angle, $\theta$ between a horizontal plane and the local neighborhood-based point normal $N$,

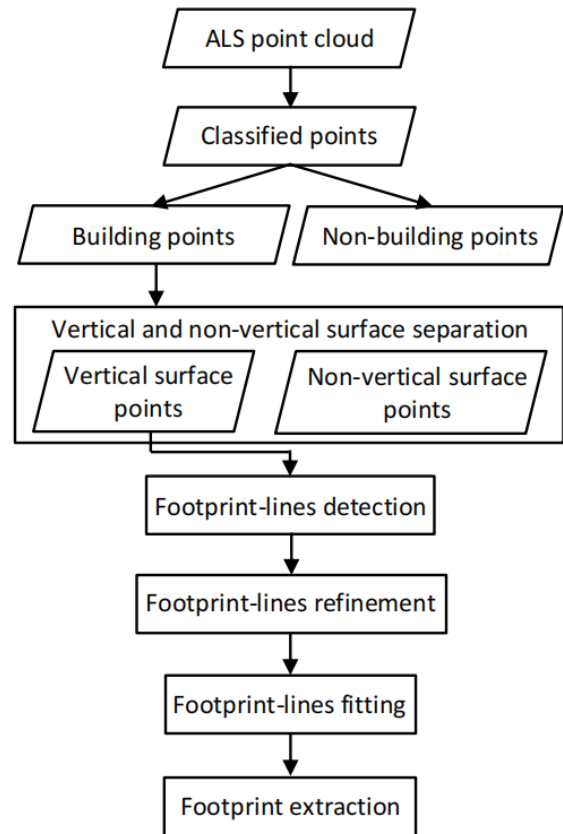$$\theta = \left| atan \frac{\sqrt{N_x^2 + N_y^2}}{N_z} \right|, \tag{6}$$



**Figure 1.** Flowchart of the proposed algorithm.

where $N_x, N_y,$ and $N_z$ are the *x*, *y*, and *z* components of the *N* of the *i*th surface point.

We use the *k* nearest neighbor (*k*NN) algorithm to get points' local neighbors. We fix an angle threshold (e.g., $70^0$ or similar) to remove the non-vertical (mainly roofs) points. The normals are estimated using the MCMD (Nurunnabi et al., 2015) algorithm, which is a robust approach for producing robust normals in the presence of noise and outliers. We remove vertical surface points from or above roofs (e.g., chimneys) using a certain height threshold $H_t$,

$$H_t = \text{median}\,(z) + c\text{MAD}\,(z), \tag{7}$$

where MAD is the median absolute deviation. Median and MAD are calculated based on the *z* (height) values. $c = 1, 2,$ or 3 that can be fixed based on the underlying data set and the building heights. We fix $c = 2$.

### 3.2 Step 2: Footprint-line detection

We know vertical surface (facades) points of a building are mainly from walls, balconies, doors, or windows. Since the ALS systems perform over the buildings, the 3D point densities of vertical facades are not sufficient for many regions (i.e., missing points/parts on the facades). Hence, we project the 3D points to the *x*-*y* plane to gain more density, and as a 2D alternative to the 3D (*x*, *y*, *z*) representation of the facades' points. Following that, we use MSAC to detect the lines from the 2D points, assuming that the building walls are straight.

### 3.3 Step 3: Spatial segmentation and footprint-lines refinement

MSAC can produce redundant (false) lines (Fig. 2) within a very close range to others, and sometimes make a single line when the points on the line are too far to lie on the same line. We use 2D spatial segmentation to separate if the Euclidean distances ($E_d$) between the points are unusual (e.g., more than 2m, depending on data density). We define a safeguarded area, fix an angle threshold ($A_t$, e.g., $5^0$), and a threshold for the minimum number of points ($nPT=10$) to be an individual line. A line is removed if it has an angle less than the threshold $A_t$ with its neighboring larger line, or consists of points less than $nPT$. Sometimes, small lines are disjoint mainly because of data gaps, we merge them if they are spatially close, e.g., within 2m (depending on data density) of distance. Moreover, noise or outlying points within the MSAC error boundary can produce small lines (magenta line in Fig. 2).
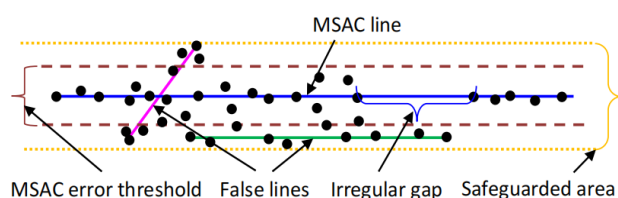


**Figure 2**. MSAC line (blue), redundant (false) lines (green and magenta). Black dots are surface points.

### 3.4 Step 4: Final footprint-lines fitting

After getting the final MSAC lines from Step 3, we fit the robust LTS regression (Rousseeuw and Leroy, 2003; Nurunnabi et al., 2016a) lines to the points used in the final MSAC-based lines. LTS is used to evade the influence of noise and outlying points that may come with extracted lines in Step 3. Hence, LTS-based footprint-lines are robust in the presence of noise and outliers.
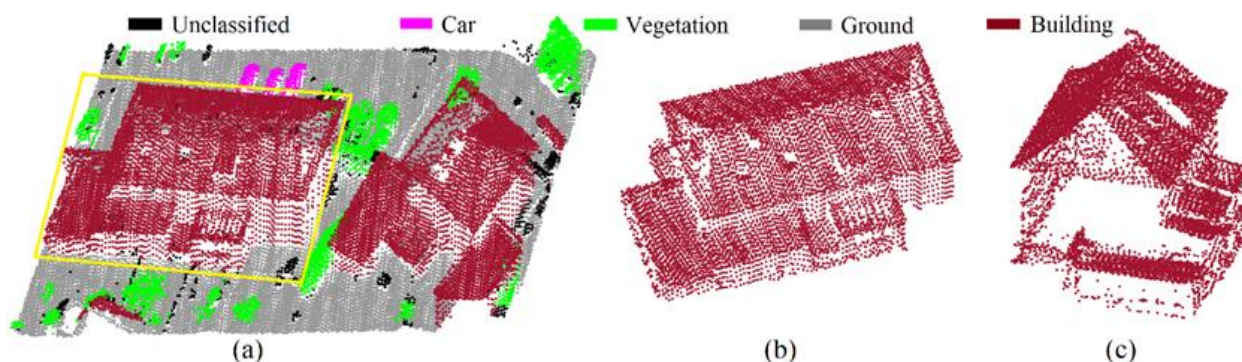
### 3.5 Step 5: Footprint extraction

We order the footprint lines and determine the intersect points of the neighboring LTS lines to get the corner points of the lines. We draw the lines to show the final footprints, join the lines using corner points and leave gaps where corner points are not available. Finally, we recheck and extract the points that are close to the ground surface points and belong to the facades.

## 4. EXPERIMENTS, ANALYSIS AND EVALUATION

This section demonstrates the new algorithm through two real-world ALS data sets.

### 4.1 Experiments on the Dudelange data set

For the first experiment, we consider a data set provided by the Administration du Cadastre et de la Topographie (ACT) of Luxembourg. The data set (Fig. 3a) is of a semi-urban area, Dudelange, Luxembourg having an average point density of $15/m^2$. The points are labelled as: ground, vegetation, buildings, cars, and unclassified using the RandLA-Net algorithm. Minor manual editing was performed to obtain more accurate building points (Fig. 3b, c). We performed our algorithm as described in Section 3 for the building in Fig. 3b. Results are depicted in Fig. 4. Points' normals are estimated based on the MCMD approach, we employ the $k$NN algorithm with $k = 30$ to get local neighbors. Robust normals for each and every point of the building were used to calculate the slope, $\theta$ values in Eq. (6). We separate the vertical ($\theta > 70^0$) and non-vertical ($\theta \leq 70^0$) surface points, Fig. 4a. We get many vertical surface points (green) over the roof that are indicated within the yellow ellipses are mainly of Chimneys. In Fig. 4b, these vertical points over the roof are eliminated using the formula stated in Eq. (7). The vertical points are mainly from the building walls projected onto the $x$-$y$ plane; we get the 2D points in Fig. 4c. The points accumulate some rectangular or polygonal shapes. We use MSAC to find straight lines for the 2D points. There are many redundant or false lines (red) in Fig. 4d that are very close to each other, or falsely identified based on the points from different regions (walls), or as the effect of the presence of noise and outliers. For example, points in the green ellipses in Fig. 4c cause for pseudo-outliers that are responsible for the false line that appeared in the green leaf in Fig. 4d. To remove the false lines, we follow the rules of spatial segmentation as mentioned in Section 3.3; distance between two consecutive points in a line would be less than 2m, and the conditions based on the angle threshold ($A_t$) is of less than $5^0$, and the minimum number of points $nPT = 10$ to be an individual line. Results of spatial segmentation and elimination of redundant lines are in Fig. 4e and 4f, respectively. We fit LTS regression lines to the points after eliminating the false lines (Fig. 4g). Intersect points are calculated for the ordered lines, and lines are drawn accordingly to get the final outlines (Fig. 4h) of the building footprints. Fig. 4i shows that the new algorithm successfully extracts building footprints that are perfectly aligned to the manually defined ground-truth of the 3D building in Fig. 3b, c.



**Figure 3**. (a) Labelled Dudelange, Luxembourg data, (b) front-view of the building within the yellow box in plot (a) to extract footprint, (c) side-view of the building.
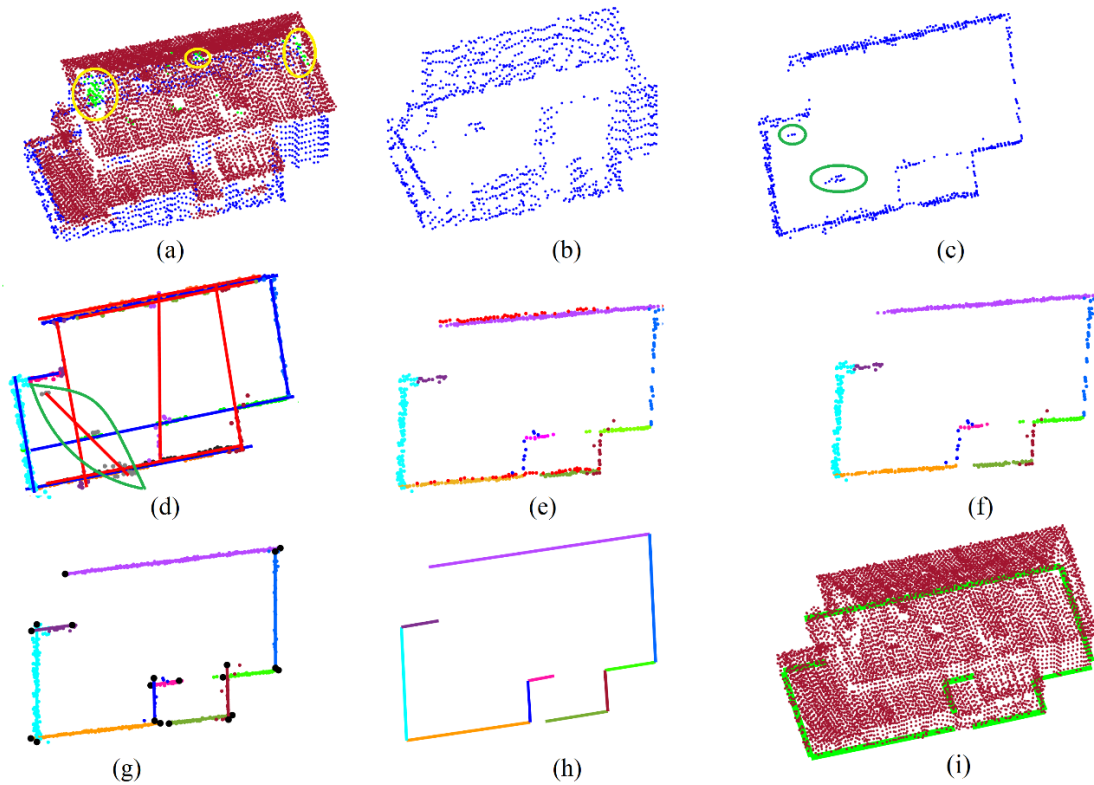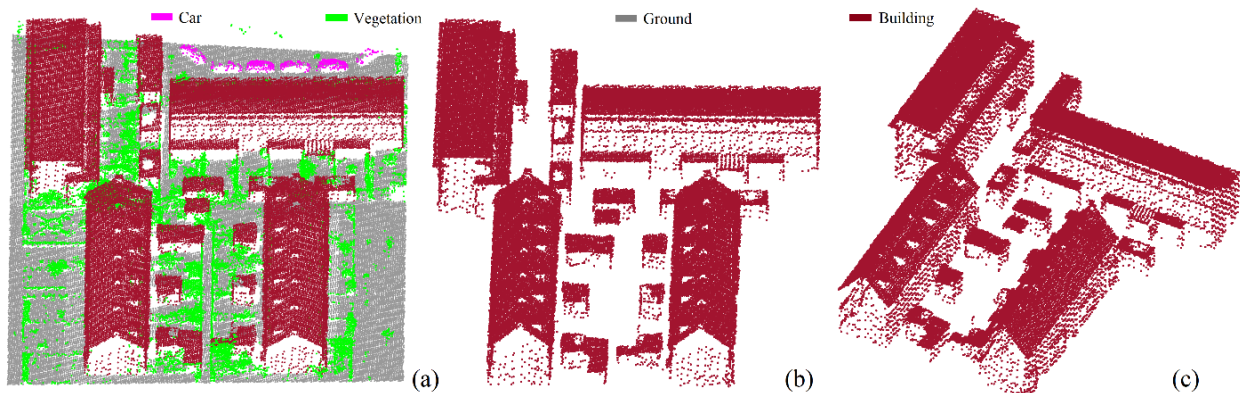
**Figure 4.** Building footprint extraction for the Dudelange data set: (a) classification of vertical (blue) and non-vertical (maroon) surfaces, vertical points within yellow ellipses are over the roof; where $\theta > 70^0$, (b) vertical surfaces (facades) below the roof, (c) 2D $(x, y)$ points for the facades, (d) extracted lines using MSAC, (e) spatial segmentation for the 2D facades points; $E_d = 2$m, (f) elimination of the redundant lines; using $A_t = 5^0$, $n$PT=10, (g) LTS regression lines, (h) footprint-lines for the building, and (i) footprint (green)-lines aligned with the 3D building's ground-truth.

## 4.2 Experiments on the AHN data set

The second experiment was performed using the open access Actueel Hoogtebestand Nederland (AHN) data of the Netherlands. The data set (Fig. 5a) is of an urban area having 83,517 points with an average point density of around 20/m². Although, the data set is available with respective points' labels of ground, vegetation, and building, we performed the RandLA-Net algorithm and some manual editing to get accurate segmentation including car points. This manual editing helps us to understand the ground truth. This data set has 4 large buildings, and 13 small buildings that have 85 walls in total, including 82 exterior walls, among them 69 exterior walls have points. We see many of the walls for the buildings are partially

scanned or totally missed especially on the opposite side of the scanner, see Fig. 5b, and c.

We performed the proposed algorithm on the identified building points. Results are portrayed in Fig. 6. The necessary parameters were set similarly to the previous experiment. Points normals are estimated based on the MCMD algorithm. The slope, $\theta$ values for each and every point of the buildings were calculated. The vertical (blue) and non-vertical surface points mainly from roofs (maroon) are separated (Fig. 6a), using the angle threshold of $\theta = 70^0$, as in the first experiment, hence the vertical points have slopes greater than $70^0$. Vertical surface points over the roofs were removed using the height threshold and the formula defined in Eq. (7).



**Figure 5.** (a) Labelled AHN data set, (b) front-view of the buildings to extract footprint, (c) side-view of the buildings.
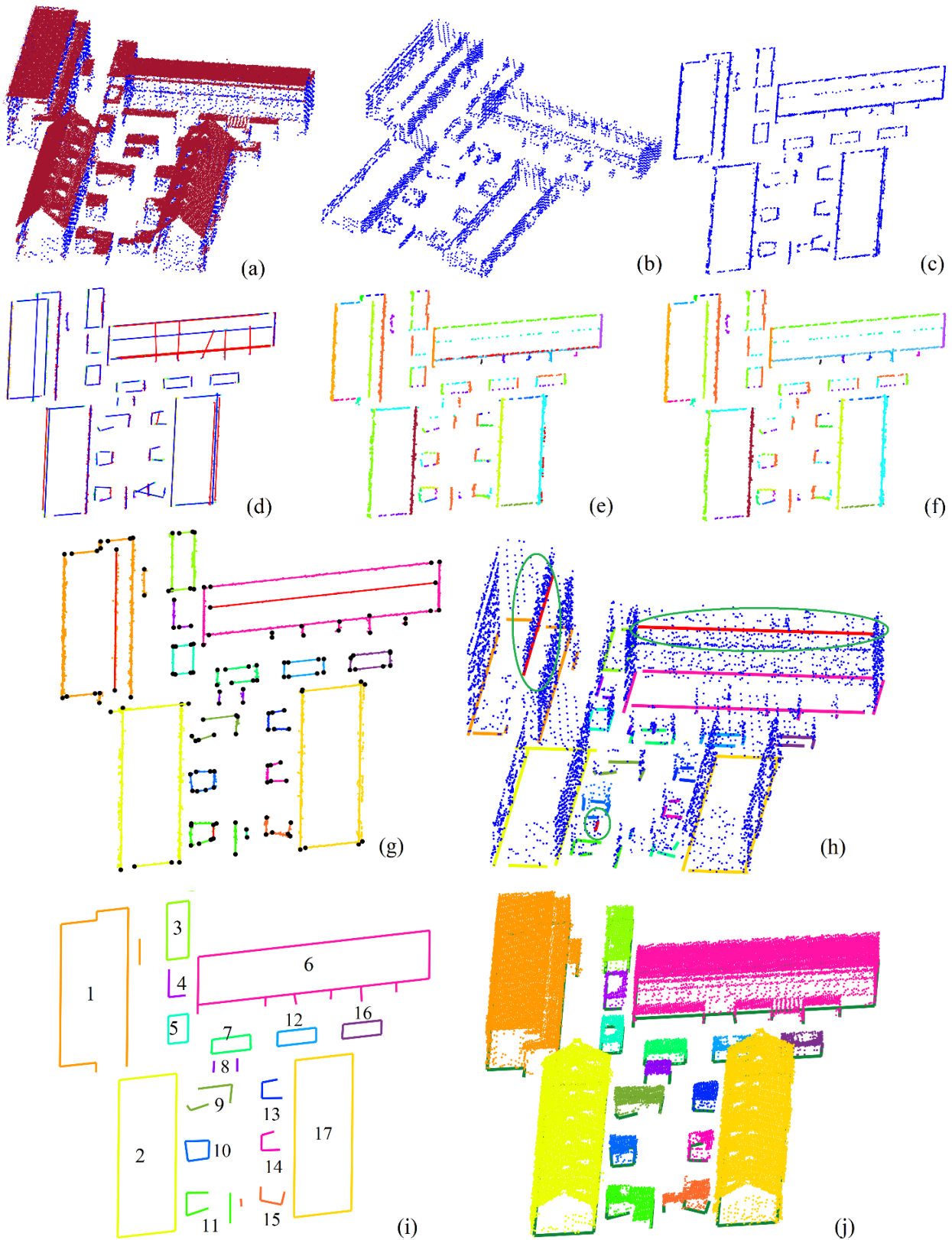
**Figure 6.** Building footprints extraction of AHN data set: (a) classification of vertical (blue) and non-vertical (maroon) surfaces, (b) 3D vertical surfaces (facades) below the roofs, (c) 2D (*x*, *y*) points for the vertical surfaces, (d) extracted lines using MSAC for the points in plot (c), (e) spatial segmentation for the 2D facades points in plot (d), (f) elimination of redundant/false (red) lines in (e); using $A_t = 5^0$, and $n$PT=10, (g) LTS regression lines for the points in plot (f); black dots are the end points of the lines, (h) footprint-lines for the buildings in 3D, red lines within the three green ellipses are from the hanging walls that have no ground connection, (i) final footprint-lines for the buildings, and (j) footprint (green)-lines aligned with the 3D buildings in plot (a).

| Building sl. number | Ground truth | | | No. of exterior walls where points are available | Extracted footprint | | Building sl. number | Ground truth | | | No. of exterior walls where points are available | Extracted footprint lines | |
|---|---|---|---|---|---|---|---|---|---|---|---|---|---|
| | Total walls | Interior walls | Exterior walls | | Interior walls | Exterior walls | | Total walls | Interior walls | Exterior walls | | Interior walls | Exterior walls |
| 1 | 10 | 1 | 9 | 8 | 1 | 8 | 10 | 4 | 0 | 4 | 4 | 0 | 4 |
| 2 | 4 | 0 | 4 | 4 | 0 | 4 | 11 | 7 | 1 | 6 | 4(1 partial) | 1 | 4 (1 partial) |
| 3 | 4 | 0 | 4 | 4 | 0 | 4 | 12 | 4 | 0 | 4 | 4 | 0 | 4 |
| 4 | 4 | 0 | 4 | 2 | 0 | 2 | 13 | 4 | 0 | 4 | 3 | 0 | 3 |
| 5 | 4 | 0 | 4 | 4 | 0 | 4 | 14 | 4 | 0 | 4 | 3 | 0 | 3 |
| 6 | 10 | 1 | 9 | 9 | 1 | 9 | 15 | 6 | 0 | 6 | 2 | 0 | 4(2 roof edges) |
| 7 | 4 | 0 | 4 | 4 | 0 | 4 | 16 | 4 | 0 | 4 | 4 | 0 | 4 |
| 8 | 4 | 0 | 4 | 2 | 0 | 2 | 17 | 4 | 0 | 4 | 4 | 0 | 4 |
| 9 | 4 | 0 | 4 | 4 (2 partial) | 0 | 4 (2 partial) | | | | | | | |
| C. total | 48 | 2 | 46 | 41 | 2 | 41 | | 37 | 1 | 36 | 28 | 1 | 30 |
| G. total | | | | | | | | 85 | 3 | 82 | 69 | | 71 |

**Table 1**. Buildings-wise distribution of extracted footprint-lines, the information relates to Fig. 6i. Column-wise total and Grand total are mentioned as C. total and G. total, respectively. # partial means that # walls are partially scanned.

The vertical facades (walls, Fig. 6b) points were projected onto the x-y plane; producing the 2D points in Fig. 6c that appear in some combinations of straight lines. We use MSAC to extract straight lines from the 2D points. There are many lines that are very close to each other and should be a single line. It is reasonable that they are redundant (red, in Fig. 6d) to represent a single facade. Actually, they are falsely identified based on the points from different regions (walls), or as the effects of the presence of noise and outliers. Generating lines that are very close to each other mainly due to the limitation of RANSAC type algorithms; if the threshold for considering inliers is not perfectly fixed (Torr and Zisserman, 2000). To remove the false lines, we follow the rules of spatial segmentation used in the first experiment, described in Section 3.3. Besides, we used the conditions based on the angle threshold ($A_t = 5^0$), and the minimum number of points ($n$PT=10) to get individual lines. Results of spatial segmentation and elimination of false and/or redundant lines by using $A_t = 5^0$, and $n$PT=10 are shown in Fig. 6e and f, respectively. Fig. 6g shows the fitted LTS regression lines to the points after eliminating the false (red) lines in Fig. 6e and f. Black dots are the end points of the respective lines. Intersect points are calculated by the ordered lines, and lines are drawn accordingly to get the final polygonal outlines (Fig. 6i) of the buildings' footprints. Fig. 6j shows that the new algorithm successfully extracts building footprints that are perfectly aligned to the 3D ground-truth of the buildings in Figs. 5b, c, or 6a.

Table 1 shows the building-wise distribution of the extracted footprint-lines. It depicts that all (69) the footprint-lines are perfectly extracted, where points are available for the exterior walls. Only two lines are overly extracted for the 15th building where two roof edges were falsely included as exterior walls.

## 5. DISCUSSION AND CONCLUSIONS

We present a novel approach for building footprint extraction using ALS point cloud data. The new algorithm combines robust techniques MCMD, MSAC and LTS regression for normal estimation, footprint-line extraction, and fitting, respectively. This algorithm is robust in the presence of noise and outliers in the data. It precisely extracts building footprints based on the buildings' exterior walls (vertical facades) information. Since it uses buildings' exterior wall information rather than roofs' information, it can avoid the overestimation of the building area that could happen by using roof-based methods. Moreover, since the algorithm does not use roof information, it could avoid the problems due to the existence of structured or unstructured roofs. ALS often collects building facades with very low point density and most of the time facades are imprecise, and partially scanned that are not sufficient to get their footprints and outline. In this algorithm, using the idea of projecting 3D facades' points onto the x-y plane gives benefits to the algorithm to get more point density in terms of 2D. The 2D points that are alternative to the 3D facades look like straight lines and produce vertical precision. In the proposed algorithm, we consider several parameters that can be fixed based on the empirical study of the data available to the user. However, we see some parameters can be fixed earlier to get expected results for most of the data sets having different point densities, e.g., angle threshold and the threshold for verticality estimation are fine with the values of $A_t = 5^0$ and $\theta = 70^0$, respectively.

The experimental results based on the two datasets used in Section 4 demonstrate that combining different robust approaches (MCMD, MSAC and LTS regression) produces robust and reliable results that align with the reference boundaries of the buildings. In future work, we will incorporate point clouds and associated aerial imagery to explore color information, more point density and finally to have complete facades that can improve the footprint extraction.

## REFERENCES

ACT (Dudelange) data: https://data.public.lu/en/datasets/lidar-2019-releve-3d-du-territoire-luxembourgeois/

AHN3: Actueel Hoogtebestand Nederland data: https://app.pdok.nl/ahn3-downloadpage/

Awrangjeb, M., Lu, G., 2014. Automatic building footprint extraction and regularisation from LIDAR point cloud data. *Int. Conf. Digital Image Computing: Tech. and Appl.* (DICTA), 25–27 Nov. 2014, Wollongong, Australia.

Balado, J., Diaz-Vilarino, L., Arias, P., Gonzalez-Jorge, H., 2018. Automatic classification of urban ground elements from mobile laser scanning data. *Autom. Constr.*, 86: 226–239.

Buyukdemircioglu, M., Can, R., Kocaman, S., Kada, M., 2022. Deep learning-based building footprint extraction from very high resolution true orthophotos and NDSM. *ISPRS annals of the Photogramm. Remote Sens. and Spat Info. Sci.*, Vol. V-2., 211–218.

Campbell, J. B., Wynne, R. H., 2011. *Introduction to Remote Sensing*. Guilford publications, NY.

Chen, M., Feng, A., McAlinden, R., Soibelman, L., 2020. Photogrammetric point cloud segmentation and object information extraction for creating virtual environments and simulations. *J. Manage. Eng.*, 36(2): 04019046.

Choi, S., Kim, T., Yu, W., 2009. Performance evaluation of RANSAC family. *BMVC*, London, UK, September 7–10, 2009.

Dalitz, C., Schramke, T., Jeltsch, M., 2017. Iterative Hough Transform for line detection in 3D point clouds. *Image Process. Line*, 7: 184–196.

Dimitrov, H., Petrova-Antonova, D., 2021. 3d city model as a first step towards digital twin of Sofia city. *Int. Arch. of the Photogramm. Remote Sens. and Spat Info. Sci.*, Vol. XLIII-B4, 23–30.

Ebrahimi, S. M., Arefi, H., Veis, H R. 2017. Aerial imagery and lidar data fusion for unambiguous extraction of adjacent level-buildings' footprints. *Int. Arch. of the Photogramm. Remote Sens. and Spat Info. Sci.,* Vol. XLII-4/W4. 179–183.

Fischler, M. A., Bolles, R., 1981. Random sample consensus: a paradigm for model fitting with applications to image analysis and automated cartography. *Communications of the ACM*. 24(6): 381–395.

He, K., Gkioxari, G., Dollár, P., Girshick, R., 2017. Mask R-CNN. *IEEE ICCV*, 2961-2969.

Hu, Q., et al., 2020. RandLA-Net: Efficient semantic segmentation of large-scale point clouds. *CVPR*, 11108–11117.

Mohamed, S. A., Mahmoud, A. S., Moustafa, M. S., Helmy, A. k., Nasr, A. H., 2022. Building footprint extraction in dense area from LiDAR data using Mask R-CNN. *Int. J. Advanced Computer Sci. App.*, 13(6), 346–353.

Neidhert, H., Sester, M., 2008. Extraction of building ground plans from lidar data. *Int. Arch. of the Photogramm. Remote Sens. and Spat Info. Sci*, Vol. XXXVII-B2. 405–410.

Nex et al., 2013. Building footprint extraction from oblique imagery. *ISPRS annals of the Photogramm. Remote Sens. and Spat Info. Sci.*, vol. II-3/W3, 61–66.

Nurunnabi, A., Belton, D., West, G., 2012. Diagnostic-robust statistical analysis for local surface fitting in 3D point cloud data. *ISPRS Ann. Photogramm. Remote Sens. Spatial Inf. Sci.*, 1–3, 269–274.

Nurunnabi, A., Belton, D., West, G., 2014. Robust statistical approaches for local planar surface fitting in 3D laser scanning data. *ISPRS J. Photogramm. Remote Sens.*, 96: 106–122.

Nurunnabi, A., West, G., Belton, D., 2015. Outlier detection and robust normal-curvature estimation in mobile laser scanning 3D point cloud data. *Pattern Recognit.* 48(4): 1404–1419.

Nurunnabi, A., West, G., Belton, D., 2016a. Robust locally weighted regression techniques for ground surface points filtering in mobile laser scanning 3D point cloud data. *IEEE Trans. Geosci. Remote Sens.* 54(4): 2181–2193.

Nurunnabi, A., Belton, D., West, G., 2016b. Robust segmentation for large volumes of laser scanning three-dimensional point cloud data, *IEEE Trans. Geosci. Remote Sens.* 54(8), 4790–4805.

Nurunnabi, A., Teferle, N., Li, J., Lindenbergh, R., Hunegnaw, A., 2021. An efficient deep learning approach for ground point filtering in aerial laser scanning point clouds. *Int. Arch. of the Photogramm. Remote Sens. and Spat Info. Sci.*, Vol. XLIII-B1. 31–38.

Park, Y., Guldmann, J-M., 2019. Creating 3D city models with building footprints and LIDAR point cloud classification: A machine learning approach. *Comput. Environ. Urban Syst.*, 75: 76–89.

Qi, C.R., Su, H., Mo, K., Guibas, L.J., 2017. Pointnet: Deep learning on point sets for 3d classification and segmentation. *IEEE CVPR*, 652–660.

Rau, J-Y., Lin, B-C., 2011. Automatic roof model reconstruction from ALS data and 2D ground plans based on side projection and the TMR algorithm. *ISPRS J. Photogramm. Remote Sens.*, 66: S13–S27.

Rousseeuw, P. J., Leroy, A. M., 2003. *Robust Regression and Outlier Detection*. Wiley & Sons, NY.

Schuegraf, B., Bittner, K., 2019. Automatic building footprint extraction from multi-resolution remote sensing images using a hybrid FCN. *ISPRS Int. J. Geo-Info.*, 8, 191, 1–16.

Sun, X., Zhao, W., Maretto, R. V., Persello, C., 2021. Building outline extraction from aerial imagery and digital surface model with a frame field learning framework. *Int. Arch. of the Photogramm. Remote Sens. and Spat Info. Sci*, Vol. XLIII-B2, 487–493.

Thomas, H., Qi, C. R., Deschaud, J. E., Marcotegui, B., Goulette, F., Guibas, L. J., 2019. KPConv: Flexible and deformable convolution for point clouds. *IEEE Int. Conf. Computer Vision*, 6411–6420.

Torr, P. H. S., Zisserman, A., 2000. MLESAC: A new robust estimator with application to estimating image geometry. *Computer Vision and Image Understanding*, 78:138–156.

Widyaningrum, E., Gorte, B., Lindenbergh, R., 2019, Automatic building outline extraction from ALS point clouds by ordered points aided Hough Transform. *Remote Sens.*, 11, 1727, 1–29.

Yang, B., Wei, Z., Li, Q., Li, J., 2013. Semiautomated building facade footprint extraction from mobile LiDAR point clouds. *IEEE Geosci. Remote Sens. Lett.*, 10 (4): 766–770.

Zeng, C., Wang, J., 2013. An evaluation system for building footprint extraction from remotely sensed data. *IEEE J. Sel. Top. Appl. Earth Obs. Remote Sens.* 6(3): 1640–1652.

Zhao, W., Persello, C., Stein, A., 2021. Building outline delineation: From aerial images to polygons with an improved end-to-end learning framework. *ISPRS J. Photogramm. Remote Sens.*, 175: 119–131.